

Review

Application of Metal Halide Perovskites as Photocatalysts in Organic Reactions

Marco Corti, Sara Bonomi, Rossella Chiara, Lidia Romani, Paolo Quadrelli *  and Lorenzo Malavasi *

Department of Chemistry, University of Pavia, Via Taramelli 12, 27100 Pavia, Italy; marco.corti03@universitadipavia.it (M.C.); sara.bonomi01@universitadipavia.it (S.B.); rossella.chiara01@universitadipavia.it (R.C.); lidia.romani01@universitadipavia.it (L.R.)

* Correspondence: paolo.quadrelli@unipv.it (P.Q.); lorenzo.malavasi@unipv.it (L.M.)

Abstract: This review summarizes the current status of the application of metal halide perovskites (MHPs) as photocatalysts in organic syntheses/transformations. It is shown that the optimal and unique electronic properties of MHPs can be advantageously used in several reaction types providing pros with respect to traditional photocatalysts. While still being at infancy, such field of application of MHPs as effective photocatalysts will for sure become a central research topic in the forthcoming years, thanks also to their rich structural and chemical tunability, which may provide tailored materials for most of the envisaged organic reactions.

Keywords: perovskite; photocatalyst; organic synthesis; nanocrystals; lead-free; bulk; oxidation; alkylation; polymerization



Citation: Corti, M.; Bonomi, S.; Chiara, R.; Romani, L.; Quadrelli, P.; Malavasi, L. Application of Metal Halide Perovskites as Photocatalysts in Organic Reactions. *Inorganics* **2021**, *9*, 56. <https://doi.org/10.3390/inorganics9070056>

Academic Editors: Hiroshi Kageyama and Kazuhiko Maeda

Received: 14 June 2021

Accepted: 1 July 2021

Published: 13 July 2021

Publisher's Note: MDPI stays neutral with regard to jurisdictional claims in published maps and institutional affiliations.



Copyright: © 2021 by the authors. Licensee MDPI, Basel, Switzerland. This article is an open access article distributed under the terms and conditions of the Creative Commons Attribution (CC BY) license (<https://creativecommons.org/licenses/by/4.0/>).

1. Introduction

In nature, solar light is absorbed as storable energy in chemical bonds through a vast array of biochemical reactions (C-C, C-O, and C-N forming reactions) during the photo-synthetic process. Based on this consideration, using light to induce chemical reactions (photochemistry) is an attractive strategy involving photons as traceless and sustainable reagents to provide energy for the activation of substrates and reagents. Traditionally, photochemical reactions were performed using UV light to excite substrates. However, this approach requires high energy that can be provided by special and expensive equipment leading to unselective reactions, which are difficult to control and predict. By the development of photocatalysts activated with low-energy photons, many advances have been made in this field, leading to sustainable chemical transformation driven by visible light. Photocatalysts can induce chemical reactions through several mechanistic pathways, namely photoredox catalysis, proton-coupled electron transfer, hydrogen atom transfer, and energy transfer. These mechanisms are summarized and briefly explained in Figure 1 [1]. By the way, the photocatalytic approach for the construction of valuable chemicals is a promising technique to reach a cost-effective and efficient methodology in organic chemistry [2,3]. However, many drawbacks are related to the most common catalysts currently used, such as the expensive metals required, the need of anaerobic reaction conditions, low or moderate reaction yields, and complicated preparation protocols [3–8]. Therefore, the main challenge for the development of photocatalytic procedures in organic chemistry is to achieve easy-to-produce, low-cost, and efficient catalysts to be used in several chemical bond-forming reactions. Due to the extremely appealing photophysical properties showed by metal halide perovskites (MHPs) and exploited in photovoltaics [9], these materials represent an attractive strategy to produce valuable photocatalysts [10,11]. According to the current literature, these excellent photovoltaic performances can be attributed to the unique optoelectronic properties of MHPs [12] such as strong light absorption [13], good charge-carrier lifetimes [14], and high diffusion lengths [15]. Therefore, the investigation of perovskite photocatalytic properties for organic synthesis was inspired by their superior

optical properties [16–19]. Moreover, MHPs can also be produced in a very cost-effective manner, leading to the obtainment of versatile materials, prepared from earth-abundant and cheap starting elements [20]. Indeed, perovskites-based materials are very promising candidates as photocatalysts for organic reactions under visible light for the formation of, among others, C-C, C-N, and C-O bonds [2]. The superior optical properties of MHPs make them suitable to promote several catalytic reactions such as reduction and oxidation processes, thanks to their electronic structure, their highly tunable and narrow band gap, long carrier lifetimes and good defect tolerance. The mechanisms involved in these photocatalytic reactions using MHPs are similar to those of conventional catalysts: the visible-light generation of charge carriers occurs and then they are transferred to the reaction sites, often through the mediation of a metal or a semiconductor cocatalyst [21]. The possibility of developing low-cost, easy-to-produce, highly efficient, and tunable MHPs-based photocatalysts may bring new and promising tools in chemical synthesis and organic reactions. For these reasons, in the present review, we report the current status regarding the application of MHPs photocatalysts in organic reactions, by considering the application of lead-containing and lead-free materials. For the first class, we further organized the review by summarizing the available results on bulk and nanocrystalline MHPs separately, due to the peculiar properties induced by grain size reduction on the optical characteristics and in turn on the photocatalytic activity [20,22,23].

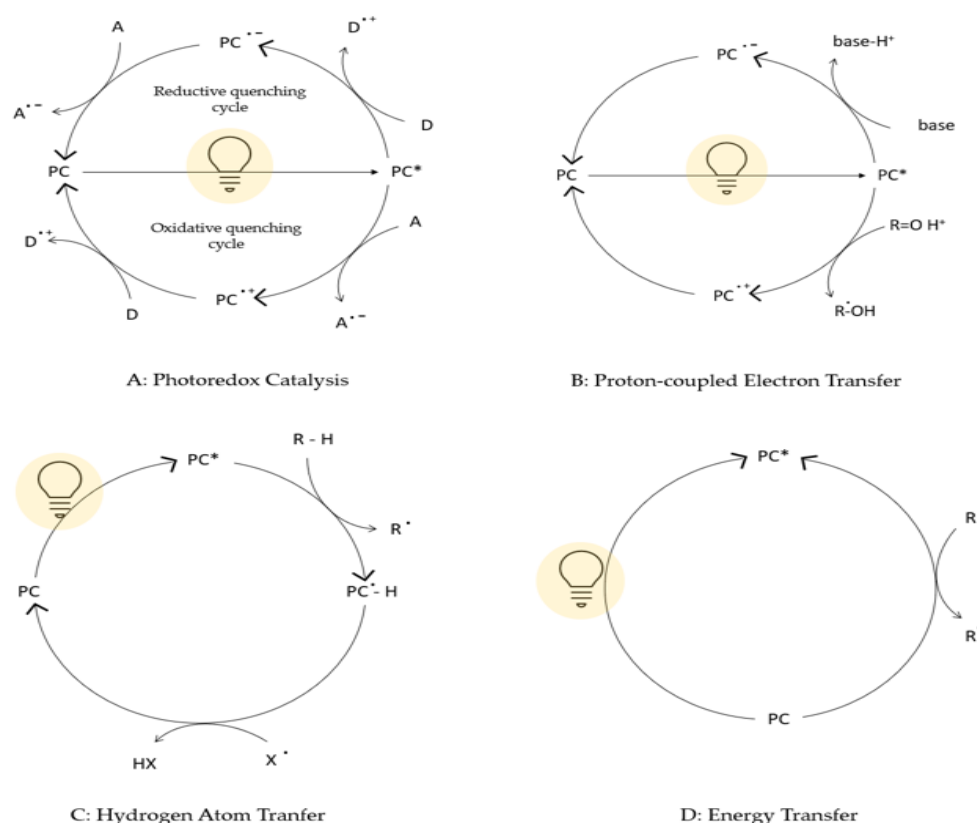


Figure 1. General mechanistic scenarios in photocatalytic synthesis. In all the pathways reported, the first step concerns the formation of an excited photocatalyst upon irradiation (PC^*). (A) Photoredox Catalysis: PC^* accepts or donate a single electron leading to oxidative or reductive quenching cycles depending on the substrates present in the reaction mixture (presence of electron acceptor or donor); (B) Proton-coupled Electron Transfer: redox events occur during a concerted proton transfer; (C) Hydrogen Atom Transfer: homolytic cleavage of C–H bonds by the photocatalyst or after singlet electron transfer events; (D) Energy Transfer: PC directly transfers its excited state energy to a substrate that normally is not able to absorb light (at the given wavelength) leading to a chemical reaction. Reprinted with permission from ref. [1]. Copyright 2021 iScience.

2. Lead-Based MHPs

The first applications of MHPs involved lead-based materials [20]. These phases are still the most employed in many fields (i.e., solar cells, LEDs, photodetectors . . .) because of their extraordinary efficiencies [20] and the almost endless possibility of tuning their structural, optical, and electrical properties playing with atomic content by changing their composition, morphology, and many others features [24,25]. For these reasons, lead-based MHPs are the most known, studied, and deeply characterized perovskites by the scientific community. Therefore, the majority of the results reported in this review refer to lead-based photocatalysts.

2.1. Nanomaterials

The high surface area of nanocrystals make them appealing for their application in photocatalysis, both for hydrogen generation [21] and organic synthesis. This led many researchers to choose MHP NCs to carry on many different organic reactions, such as the ones summarized in Table 1.

Table 1. Nanocrystalline Pb-based photocatalytic systems reviewed in the present paper highlighting the reaction, the reaction yield, and illumination means.

Catalyst		Reaction	Reaction Yield	Illumination	Reference
CsPbBr ₃	NCs	α -alkylation reaction of aldehydes	70%	Blue LED (450 nm)	[26]
CsPbBr ₃	NCs	α -alkylation reaction of aldehydes	-	-	[27]
CsPbBr ₃ MAPbBr ₃	NCs	α -alkylation reaction of aldehydes	96%	Blue LED (455 nm)	[11]
CsPbBr ₃	NCs	C-C bond formation via C-H activation N-heterocyclization C-O cross-coupling	Up to 85% Up to 90% Up to 85%	Blue LED (455 nm)	[2]
CsPbBr ₃	NCs	C-C coupling	Up to 83%	447 nm	[28]
CsPbBr ₃	NCs	aminomethylation of imidazo-fused heterocycles	Up to 94%	White LED	[29]
CsPbX ₃ (X = I, Br, Cl)	NCs	oxidative coupling of thiols phosphonylation of tertiary amines	Up to 98% Up to 96%	White LED	[19]
Bz _{0.5} PbI ₃	covered with nanometric silane layer	cis-to-trans isomerization of stilbene	Up to 100%	Xe lamp ($\lambda > 450$ nm)	[30]
CsPbBr ₃	NCs supported onto TiO ₂	benzyl alcohol oxidation	50%	Xe lamp ($\lambda > 420$ nm)	[31]
CsPbBr ₃	NCs supported onto TiO ₂	toluene oxidation	-	Xe lamp ($\lambda > 420$ nm)	[32]
FAPbBr ₃	NCs supported onto TiO ₂	benzylic alcohols oxidation	Up to 63%	Simulated solar light	[33]
FAPbBr ₃	NCs supported between NiO and TiO ₂	Csp ³ -H bond activation in cycloalkanes and aromatic alkanes	Up to 1.02%	Simulated solar light	[34]
CsPbBr ₃ /Cs ₄ PbBr ₆	Nanosheets	oxidation of styrene	-	White LED	[35]
CsPbI ₃	NCs	polymerization of TerEDOT	-	Simulated solar light	[17]
CsPbX ₃ (X = I, I _{0.67} Br _{0.33} , I _{0.5} Br _{0.5} , I _{0.33} Br _{0.67} , Br)	NCs	polymerization of TerEDOT	-	Xe lamp	[36]
CsPbBr ₃	NCs	PET-RAFT polymerization	Up to 97%	Blue LED	[37]

In the work of Lu et al., CsPbBr₃ nanocrystals (NCs) have been employed as photocatalysts for the α -alkylation reaction of aldehydes [26]. The NCs show orthorhombic structure and cubic morphology with an average size of 11.2 nm. In comparison to previous syntheses, in this work, amine-ligands were not used for the passivation of the NCs, while novel cinnamate ligands have been used for the NCs capping to increase the electron-donating

ability of CsPbBr₃ [26]. The use of such ligands allowed a relatively high photoluminescence quantum yield (PLQY) up to 70%. The authors explored different functionalized cinnamic acid (CA) ligands and found that trans-cinnamate and trans-3,5-difluorocinnamate provided the best colloid stability. These two capping agents allow also the dissolution of the NCs in polar solvents (such as methyl acetate and dichloromethane) and affect the PLQY [26]. The influence of the series of novel ligands on the NCs photocatalytic reactivity in the α -alkylation of the 3-phenylpropionaldehyde with 2-bromoacetophenone, in comparison with the more common oleic acid (OA), was therefore investigated. The CA-capped NCs present a slower reaction rate in the first minutes, followed by a higher reaction activity with respect to the OA-capped NCs, probably due to an increase of the band edge position resulting in a faster quenching of the NCs PL [26].

Wang et al. also performed an α -alkylation reaction of aldehydes using CsPbBr₃ NCs as photocatalyst [27]. In this work, an amine-free method was employed for the colloidal NCs synthesis to avoid unwanted charge transfer (CT) to the aminic ligand.

Similarly to previous reports, the synthesized NCs revealed an orthorhombic phase and an average diameter of 10 nm. The authors studied the reaction between 2-bromoacetophenone and octanal with the aid of the CsPbBr₃ NCs as catalyst and dicyclohexylamine as co-catalyst in a basic environment [27]. The co-catalyst employment allowed the reaction to proceed through a very fast mechanism (Figure 2a), which involves the electron transfer from CsPbBr₃ to 2-bromoacetophenone, and the hole transfer to an in-situ formed enamine, with the formation of two carbon-radicals that later react and form the C-C coupling product [27]. It should be highlighted that this mechanism was faster than previously reported paths employing a molecular photocatalyst (Ru(bpy)₃²⁺), as a consequence of the improved lifetime of the charge-separated state promoted by heterogeneous catalysts [27].

Zhu et al. investigated the selectivity of the C-C bond formation reactions photocatalyzed by colloidal suspensions of APbBr₃ (A = Cs, methylammonium (MA)) [11]. NCs with cubic morphology and size ranging from 2 to 100 nm have been exploited. The authors focused on the selection of the α -alkylation product, among the possible C-C coupling products, in the same reaction mentioned above, i.e., between 2-bromoacetophenone and octanal [27]. The un-catalyzed reaction generates several compounds, including dehalogenated acetophenone (yield 76%), sp³ C-coupling product (yield 8%), and α -alkylation product (yield 7%). Adding the nanocrystalline CsPbBr₃ catalyst and different molecular co-catalysts, Zhu et al. could achieve a 96% yield of the desired product (α -alkylation one) [11]. Similar results have been obtained by employing MAPbBr₃ NCs as catalysts, but with reduced stability of these NCs in organic solvents [11].

The same authors investigated other kinds of organic reactions involving cubic 2–100 nm CsPbBr₃ NCs as catalysts, such as C-C bond formation via C-H activation, N-heterocyclization, and C-O cross-coupling mechanisms [2]. They proposed as well a correlation between the NCs size and the reaction parameters, finding out that, in general, NCs with a small size promote a faster reaction rate, probably due to the higher surface area-to-volume ratio, but not necessarily a higher yield; in contrast, larger size NCs provide higher yields but a longer reaction time [2].

Rosa-Pardo et al. described for the first time the reaction between DIPEA (*N,N*-diisopropylethylamine) and benzyl bromides, catalyzed by CsPbBr₃ NCs, for the formation of C-C coupling products [28]. In this reaction (Figure 2b), DIPEA acts as an electron donor and enables the electron transfer from CsPbBr₃ to the benzyl bromide, which later reacts forming a C-C bond [28]. The authors used various *p*-substituted benzyl bromides as substrates and found out that the product yield depends on the nature of the *p*-substituent (H, *t*BU, OMe > Cl > Br) [28].

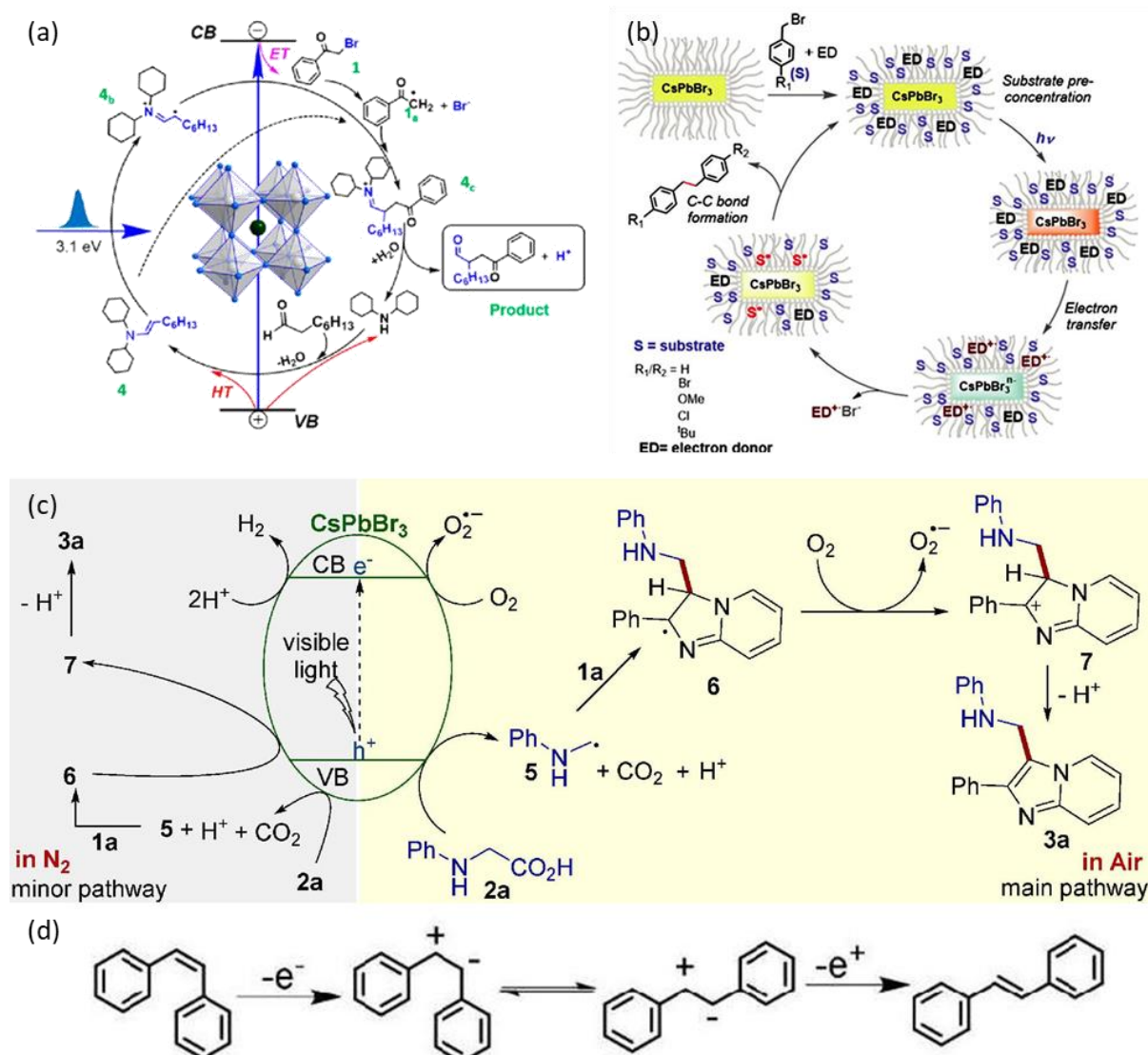


Figure 2. Proposed reaction mechanisms: (a) for the α -alkylation catalyzed by CsPbBr₃ NCs. For details, see ref. [27]. Reprinted with permission from ref. [27]. Copyright 2020 ACS Energy Letters. (b) for the coupling reaction, through cooperative action between the NC surface and the ligand. For details, see ref. [28]. Reprinted with permission from ref. [28]. Copyright 2020 ChemComm. (c) for the decarboxylative coupling reaction. For details, see ref. [29]. Reprinted with permission from ref. [29]. Copyright 2020 Adv. Synth. Catal. (d) for the photocatalytic cis-to-trans stilbene isomerization. For details, see ref. [30]. Reprinted with permission from ref. [30]. Copyright 2019 ChemCatChem.

Shi et al. focused on the photocatalytic activity of 50 nm CsPbBr₃ crystals in the aminomethylation of imidazo-fused heterocycles [29]. The reaction occurs via decarboxylative coupling of *N*-phenylglycines with imidazo-fused heterocycles under the irradiation of visible light. The authors selected imidazo[1,2-*a*]pyridine (1a, Figure 2c) and *N*-phenylglycine (2a, Figure 2c) to start their investigation and tried to modify the reaction conditions and *N*-phenylglycine amount in order to optimize the reaction yield toward the desired product (3a, Figure 2c). They found that the presence of CsPbBr₃ (formed in situ through the addition of CsBr and PbBr₂) as catalyst provided the desired product with an excellent yield, while the reaction was severely inhibited when conducted in absence of perovskite [29].

Subsequently, the authors studied the same aminomethylation reactions by examining different precursors such as substituted imidazo[1,2-*a*]pyridines: in this case, the presence of an electron-donating group (-OMe, -Me) on the phenyl ring promotes a higher yield of

the desired product compared with the presence of an electron-withdrawing substituent (-F, -Cl, -Br, -CN and CF₃) [29]. A plausible mechanism for this photocatalytic reaction is reported in Figure 2c. The interesting advantage of this work is that, after the reaction, the CsPbBr₃ catalyst can be simply centrifuged, washed, dried, and then reused for the next reaction cycle; it can also be employed at least five times without a reduction in its activity [29].

Wu et al. demonstrated the photocatalytic oxidative coupling of organic thiols to disulfides and a phosphorylation of tertiary amines via visible-light-mediated cross-dehydrogenative coupling reaction using CsPbX₃ (X = halogen) NCs as photocatalysts [19]. For the first type of reaction, the authors used thiophenol as the substrate and were able to conduct oxidation under a strict oxygen-free environment in the presence of NCs with different Br/I content. The bromide-rich perovskite provided the highest reaction yield, because of its better oxidative potential compared to CsPbI₃ [19]. The reaction mechanism consists of the coordination of the thiol group to the NCs surface. The thiol S and H coordinates to Pb and Br, respectively. After the excitation, electron transfer from the perovskite conduction band to the proton and the hole transfer from the valence band to the mercaptan group occurs, generating a hydrogen radical and a thiyl radical. The former will couple to produce H₂ while the thiyl radicals couple to form the corresponding disulfides on the catalyst surface [19]. Moreover, the same catalyst has been employed for the C-H activation in the phosphorylation of N-aryl tetrahydroisoquinoline derivatives with tertiary amines, gaining excellent yields [19].

Another example of surface-functionalized perovskite for organic catalysis has been described by Peng et al. who prepared an (organo)silica-coated 1D hybrid perovskite, Bz_{0.5}PbI₃ (Bz = benzenidinium, ⁺NH₃-C₆H₄-C₆H₄-NH₃⁺) and investigated its photocatalytic activity towards the cis-to-trans isomerization of stilbene [30]. They carried out the silanization of perovskite with three different silylating agents (trimethoxy(octadecyl)silane (ODTMS), tetraethyl orthosilicate (TEOS), and triethoxy perfluorodecyl silane (TEOS)), obtaining samples with average thickness from 2 to 6 nm and enhanced hydrophobic character. After the silanization, the optoelectronic properties of the perovskite are preserved [30]. The authors observed that the photocatalytic reaction did not take place in absence of photocatalyst and found out that the cis-to-trans isomerization of stilbene occurred in presence of the silica-capped perovskites, regardless of the silylating agent used, with the coating thickness influencing the photocatalytic activity [30]. The advantage of this kind of surface modification with a coating layer is the chance to reuse the photocatalyst several times before its degradation. Figure 2d shows the proposed mechanism for the photocatalytic cis-to-trans stilbene isomerization through the intermediacy of the corresponding radical cations [30].

In addition, the possibility of creating MHP-based photocatalytic composites may bring new tools in organic synthesis, thanks to the great tunability in the band gap of MHPs allowing to modify the relative band-alignment between two semiconductors, thus taking advantage of the relative efficiencies [21].

In 2018, Schünemann et al. investigated the use of the CsPbBr₃/TiO₂ composite material for selective catalysis in a benzyl alcohol oxidation to benzaldehyde under visible-light illumination [31]. They prepared the catalyst by a simple low-temperature wet-impregnation method and achieved a theoretical perovskite NCs weight loading of 20%. The synthesized CsPbBr₃ NCs had a diameter of approximately 2–4 nm and any capping agent was necessary because of TiO₂ support restricting the perovskite NCs growth [31].

This composite material provided an excellent selectivity towards benzaldehyde (>99%). Its photocatalytic activity can be explained by the formation of a ligand-to-metal charge-transfer complex between benzyl alcohol and TiO₂. The reaction mechanism (Figure 3d) involves the formation of a superoxide radical and a cation alcoholate radical that react yielding the desired aldehyde [31].

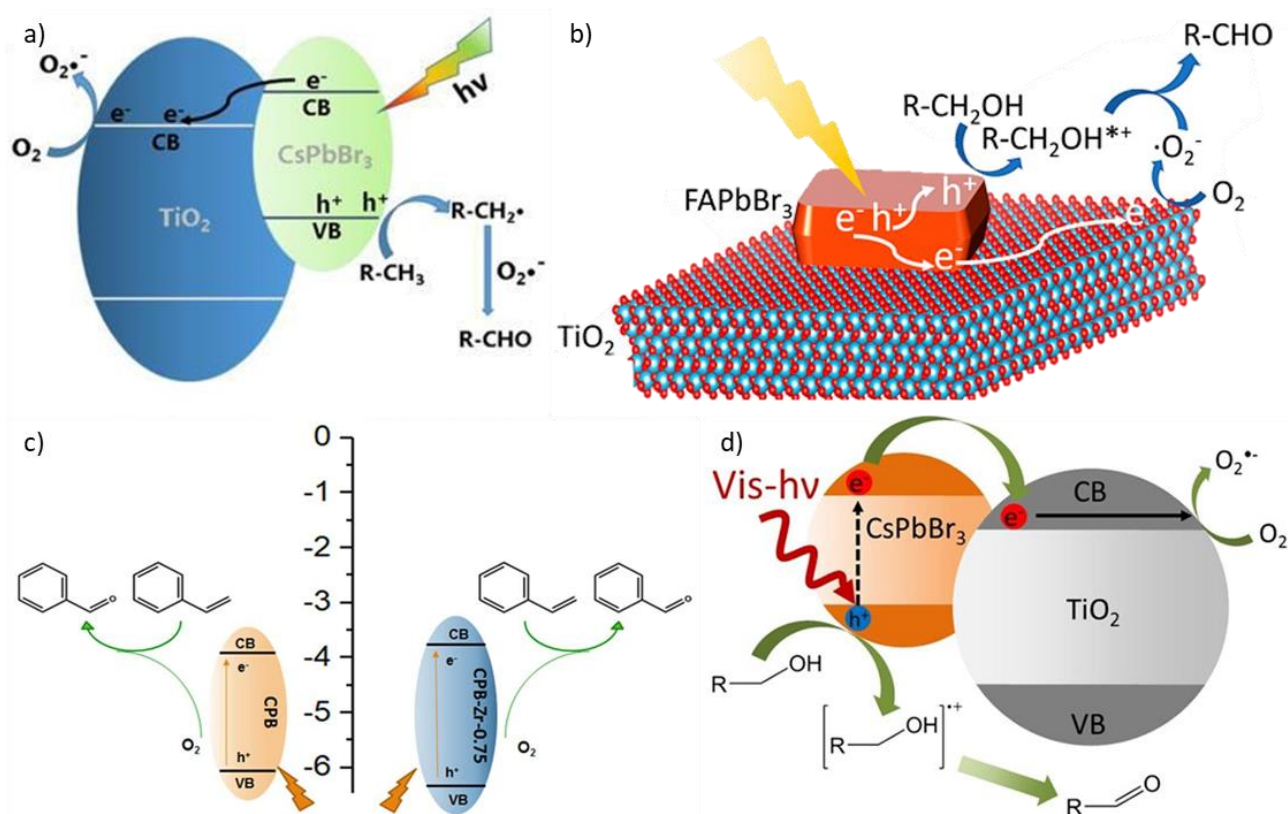


Figure 3. Proposed reaction mechanisms: (a) for the oxidation of toluene to benzaldehyde. For details, see ref. [32]. Reprinted with permission from ref. [32]. Copyright 2020 Kin. J. Chem. (b,d) for the oxidation of benzyl alcohol to benzaldehyde. For details, see refs. [31,33]. Reprinted with permission from refs. [31,33]. Copyright 2018 ACS Energy Letters. Copyright 2018 ChemSusChem. Ref. [33] is available online at: <https://pubs.acs.org/doi/full/10.1021/acscenergylett.8b00131> (Accessed on 12 July 2021) (c) for the oxidation of styrene to benzaldehyde. For details, see ref. [35]. Reprinted with permission from ref. [35]. Copyright 2020 Frontiers in Chemistry.

Two years later, Zhu et al. focused as well on the photocatalytic activity of CsPbBr₃ NCs/TiO₂ composite material for the direct oxidation of toluene into benzaldehyde (Figure 3a) [32]. CsPbBr₃ NCs have been synthesized via the ligand-assisted reprecipitation (LARP) method, obtaining irregular shapes with a sub-10 nm size and a monoclinic structure. The authors studied the photocatalytic reaction rate variation as a function of the perovskite/TiO₂ ratio. The same mechanism described above [31] occurs also in this case (Figure 3d).

Analogously, Huang et al. produced a FAPbBr₃/TiO₂ hybrid photocatalyst, which was applied for the oxidation of benzylic alcohols [33]. The authors managed to synthesize the composite material with a simple anti-solvent precipitation method, resulting in crystals of average dimensions around 180 nm with a little blue shift of the absorption edge. They prepared samples at increasing perovskite amounts (from 1% to 25%), thus increasing the absorption volume [33]. The catalyzed reaction involves an initial CT of electrons from FAPbBr₃ to TiO₂, thus oxidizing the alcohol to a carbocation by the holes that remained in the perovskite. At the same time, molecular oxygen is reduced to [•]O₂⁻. Finally, the carbocation and [•]O₂⁻ react to each other and form the corresponding aldehyde (Figure 3b) [33]. The variation of the photocatalytic performances underlines a synergic effect between TiO₂ and FAPbBr₃, resulting in a substantial increase of the benzylic alcohol to toluene conversion. In fact, while both pristine components show a conversion rate of 15%, the hybrid materials reach a maximum conversion of 63%, in particular for the sample containing 15% of MHPs [33]. A further increase in perovskite weight leads to a decrease in performance, both because the FAPbBr₃ crystals grow in dimensions, requiring the

charge carriers to travel for a longer distance and reducing the charge separation efficiency, and because the increased TiO_2 surface coverage reduces its exposed active sites [33]. In experiments carried out on benzyl alcohol and other aromatic alcohols, the authors found that this hybrid photocatalyst also exhibits a very high selectivity towards the formation of the corresponding aldehyde [33]. However, when the catalyst has been used for repeated reaction cycles, its activity is gradually decreased, probably because the perovskite slowly dissolves in the produced aldehyde, limiting the long-term stability of the system [33].

Huang et al. developed a three-component hybrid perovskite-based solar photocatalytic cell, $\text{NiO}_x/\text{FAPbBr}_3/\text{TiO}_2$, for $\text{Csp}^3\text{-H}$ bond activation in cycloalkanes and aromatic alkanes selective oxidation [34]. FAPbBr_3 NCs have been prepared in its cubic phase. The authors also tested this photocatalyst in the oxidation of toluene and substituted toluene to the respective benzaldehydes and benzyl alcohols, trying to optimize the reactions condition and the three components ratio [34].

A work published in 2020 by Qiu et al. described the fabrication of surface-functionalized $\text{CsPbBr}_3/\text{Cs}_4\text{PbBr}_6$ nanosheets (CPB) and their application as a photocatalyst in the oxidation of styrene into benzaldehyde [35]. They synthesized the surface-modified 3D/2D perovskite nanosheets with a one-pot LARP method, resulting in rectangular nanosheets with a size range of 100–400 nm. After that, ZrCl_4 was employed to modify the nanosheets to enhance the oxidation ability and to increase the production rate of benzaldehyde. The improved photocatalytic activity depends on the synergistic effect of the Cl doping and the surface functionalization with Zr species [35]. The proposed reaction mechanism is the following (Figure 3c): after the light-induced excitation inside the CPB, the electrons travel to the surface and react with adsorbed O_2 to generate activated oxygen species; meanwhile the styrene is adsorbed on the surface of the CPB and oxidized by the holes to the corresponding cationic radicals. Then the activated oxygen species oxidize the cationic radicals generating the final product [35].

Chen et al. reported the use of CsPbI_3 NCs as catalysts for the polymerization of 3,4-ethylenedioxythiophene (TerEDOT) to poly(3,4-ethylenedioxythiophene) (PEDOT) [17]. In the reaction, TerEDOT is the hole acceptor and either 1,4-benzoquinone (Qu) or molecular oxygen is the electron acceptor. The polymerization occurs with the oxidation of TerEDOT caused by the hole transfer (Figure 4a) [17]. CsPbI_3 NCs act as photocatalyst for the polymerization of the monomer and, at the same time, they are encapsulated into the polymer network. Obviously, the polymerization depends on the concentration of the NCs: a high concentration accelerates the reaction rate. If the Qu is used as electron acceptor, the perovskite maintains its starting cubic crystal structure, while, when oxygen acts as electron acceptor, the structure changes to orthorhombic [17].

Li et al. studied as well the photocatalysis of the polymerization of TerEDOT by employing Br/I alloyed CsPbX_3 ($X = \text{I}, \text{I}_{0.67}\text{Br}_{0.33}, \text{I}_{0.5}\text{Br}_{0.5}, \text{I}_{0.33}\text{Br}_{0.67}, \text{Br}$) [36]. All the NCs show a cubic morphology, with an average size of 10.6 nm. The authors verified that the catalytic activity increases with the iodine content, correlating this feature to the band gap narrowing and the exciton binding energy decrease [36]. For the NCs synthesis, the classical hot-injection method, using both amine and carboxylic ligands (OA and oleyl amine (OLA)), was performed. They also tried to replace OA with acetic acid, via treatment with methyl acetate (MeAc), obtaining an enhanced photocatalytic activity, which has been attributed to an improved CT [36].

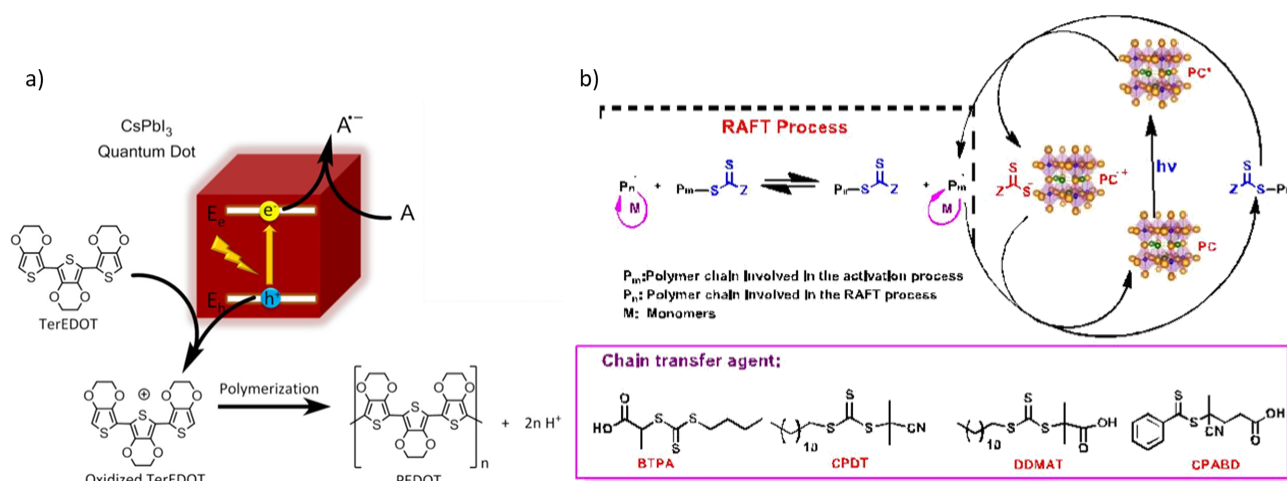


Figure 4. Proposed reaction mechanisms: (a) for the polymerization of TerEDOT over CsPbI₃ QD. For details, see ref. [17]. Reprinted with permission from ref. [17]. Copyright 2017 Journal of the American Chemical Society, available online at: <https://pubs.acs.org/doi/full/10.1021/jacs.7b06413> (accessed on 12 July 2021) (b) for the PET-RAFT polymerization. For details, see ref. [37]. Reprinted with permission from ref. [37]. Copyright 2020 ACS Macro Letters.

Another type of polymerization reaction photocatalyzed by lead halide perovskite nanocrystals was investigated by Zhu et al., who focused on the photoinduced electron/energy transfer-reversible addition-fragmentation chain transfer (PET-RAFT) polymerization [37]. The group initially employed colloidal CsPbBr₃ NCs as catalyst (cubic structure and average particle size of 11 nm) for the PET-RAFT polymerization (Figure 4b) of a methyl acrylate (MA) monomer with 2-(n-butyltrithiocarbonate) propionic acid (BTPA) acting as a chain-transfer agent (CTA) [37]. Then, different CTAs (trithiocarbonates such as 2-cyano-2-propyl dodecyl trithiocarbonate (CPDT) and 2-(dodecylthiocarbonothioylthio)-2-methylpropionic acid (DDMAT)) (Figure 4b), various monomer (butyl acrylate (BA) and 2,2,2-trifluoroethyl acrylate (TFEA)), and several monomer-to-CTA ratios have been examined to study a tuning of the degree of MA polymerization. The main result was a higher monomer conversion in the same time frame for the photopolymerization with BTPA, probably due to a more effective electron transfer between NCs and BTPA [37].

In addition, various Br/I alloyed compositions of CsPbX₃ with cubic structure have been investigated for the same PET-RAFT polymerization reactions, resulting in a decrease of monomer conversion along with the increase of the iodine content [37].

Most of the papers summarized in this section deal with CsPbBr₃ NCs. This choice is due to several reasons such as their high stability over time with respect to other phases, such as FAPbBr₃ (which also permits their deposition as thin films on substrates). Moreover, they can be obtained by a simple synthesis method [38] and the nanocrystal form of CsPbBr₃ is easier to produce than the bulk one. Lastly, these NCs are the first ones which have also been employed in other field of applications, such as in optoelectronic devices [38]. Therefore, we can affirm that CsPbBr₃ NCs have been successfully applied for efficient photocatalytic reactions, such as oxidation, alkylation, and polymerization reactions. among others. Because of their high stability and ease of production, CsPbBr₃ nanocrystals represent an appealing metal halide perovskite-based photocatalyst for the development of efficient synthetic tools.

2.2. Bulk

Despite the absence of a very high surface/volume ratio, the advantage in using bulk perovskites lies in the fact that they often overcome some problems of NCs, such as the high instability towards oxygen, moisture, and other factors which lead their decomposition. Indeed, their preparation does not require the use of anhydrous solvents and suitable

capping agents for the surface passivation and in general most of them can be prepared by easy and fast syntheses [25], as the ones listed in Table 2.

Table 2. Bulk Pb-based photocatalytic systems reviewed in the present paper highlighting the reaction, reaction yield, and illumination mean.

Catalyst	Reaction	Reaction Yield	Illumination	Reference
HDA ₂ PbI ₄ (HAD = hexadecylammonium)	Decarboxylation of indoline-2-carboxylic acid	Up to 98%	White LED	[39]
	Dehydrogenation of indoline-2-carboxylic acid	Up to 84%		
MAPbBr ₃	hydroxymethylfurfural oxidation	Up to 90%	450 nm	[40]
MAPbI ₃ FAPbI ₃ MAPbBr ₃	Conversion of triose to butyl lactate	60% 25% -	Solar light	[41]
PEA ₂ PbX ₄ (X = Br, Cl)	Supported onto C ₃ N ₄	¹ O ₂ hetero Diels-Alder cycloaddition reaction	Up to 43%	Simulated solar light [42]

Hong et al. employed HDA₂PbI₄ (HAD = hexadecylammonium) in photocatalytic decarboxylation and dehydrogenation reactions [39]. A large organic cation has been chosen to improve the perovskite stability in protic media by repulsion of the solvent molecules. Thanks to this strategy, they were able to synthesize micrometric single crystalline samples exceptionally stable in water (the Sn samples turned out less stable because of the oxidation of Sn²⁺ to Sn⁴⁺) [39].

The group employed these perovskites as photocatalysis for two different oxidation reactions (Figure 5a): the dehydrogenation and decarboxylation of indoline-2-carboxylic acid to indole or to indoline (changing the reaction conditions) [39]. For the decarboxylation, after irradiation, the perovskite acquires an electron from the precursor, with the formation of a radical species that loses the carboxylic group and acquires an H⁺ cation and an electron to form the indoline. For the dehydrogenation, after the loss of the carboxylic group, the intermediate reacts with O₂^{*−} (that is formed through the interaction with the perovskite) to form the indole [39]. In both cases, the reaction requires a hole scavenger to proceed. It also turned out that during the catalytic cycle, the perovskite underwent only minor decomposition and could be almost completely recovered and reused [39].

Zhang et al. used MAPbBr₃ as a photocatalyst in the hydroxymethylfurfural (HMF) oxidation reaction [40]. The authors carried out a solution synthesis that led to produce a crystalline powder. In the presence of MAPbBr₃ and O₂ as electron scavengers, HMF is completely oxidized and 2,5-diformylfuran (DFF) with a 90% yield is formed [40]. The group also proposed a mechanism (Figure 5c) that involves the formation of a carbo-anion intermediate that then decomposes into the desired product [40].

MAPbI₃ has been used as a photocatalyst by Dong et al. for the conversion of triose (specifically 1,3-dihydroxyacetone, DHA) and butanol to butyl lactate [41]. They used a powder with tetragonal crystal structure, with grains of average size 730 nm. The authors propose that the interaction with the perovskite allows the DHA to be oxidized to pyruvaldehyde, which in turn reacts with butanol and, through a series of keto-enolic tautomerizations, transforms to butyl lactate (Figure 5b) [41].

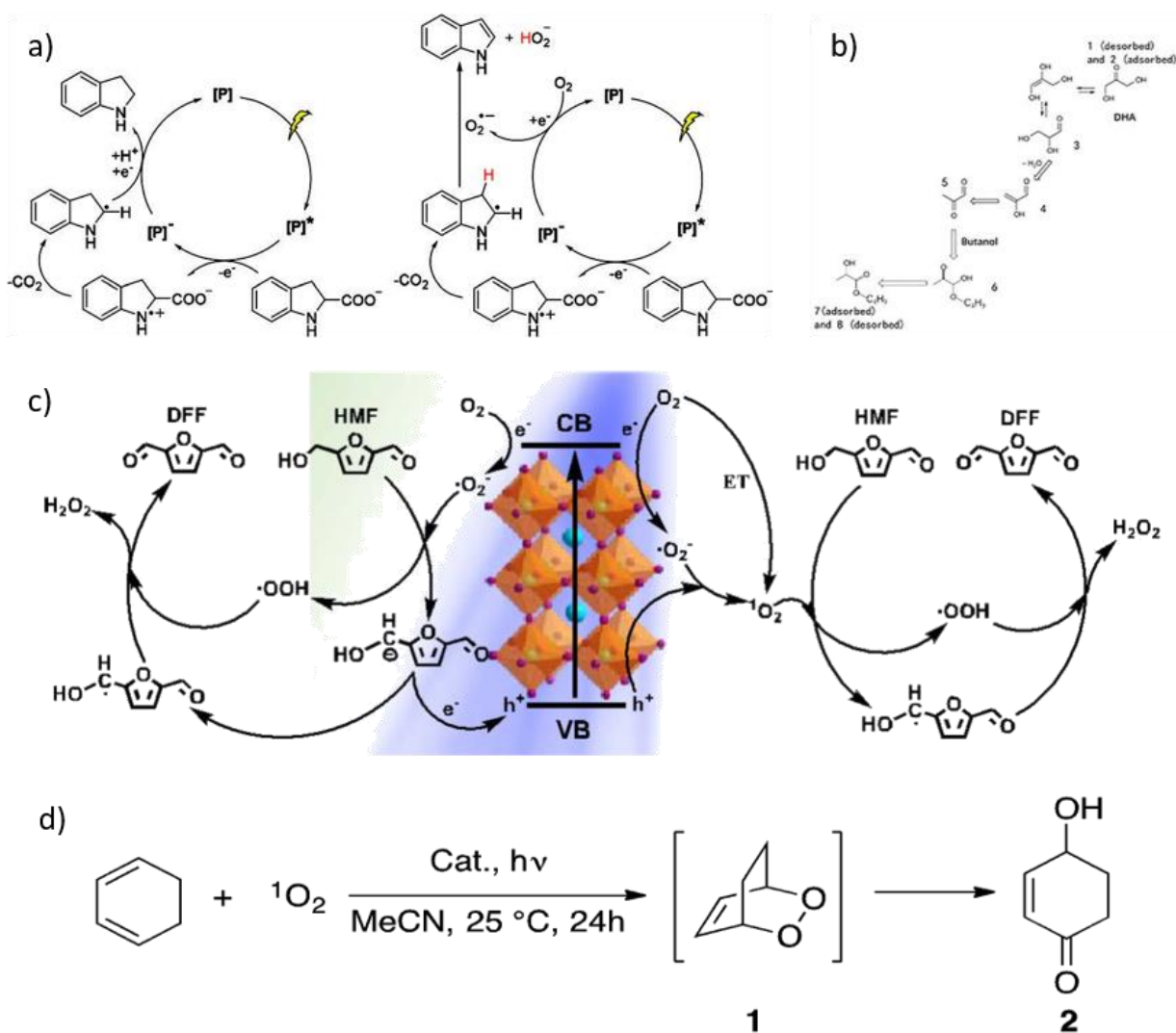


Figure 5. Proposed reaction mechanisms: (a) for the decarboxylation (left) and dehydrogenation (right) of indoline-2-carboxylic acid. For details, see ref. [39]. Reprinted with permission from ref. [39]. Copyright 2019 Angewandte Chemie International Edition. (b) for the conversion of DHA into butyl lactate. For details, see ref. [41]. Reprinted with permission from ref. [41]. Copyright 2020 Angewandte Chemie International Edition. (c) for the oxidation of HMF using MAPbBr₃ photocatalyst and atmospheric O₂. For details, see ref. [40]. Reprinted with permission from ref. [40]. Copyright 2020 ACS Catalysis. (d) for the HDA cycloaddition reaction of 1,3-cyclohexadiene and ¹O₂. For details, see ref. [42]. Reprinted with permission from ref. [42]. Copyright 2021 Catalysis Science & Technology.

In Corti et al.'s work, two different 2D lead hybrid perovskites composites (g-C₃N₄/PEA₂PbX₄; X = Br, Cl) were synthesized and characterized as photocatalysts under visible light [42]. Many different substrates such as dienes, alkenes, and aromatic compounds were considered to synthesize valuable oxidized chemicals. In particular, a ¹O₂ hetero Diels-Alder cycloaddition reaction with 1,3-cyclohexadiene (Figure 5d) was used as a benchmark reaction for the characterization [42].

According to the results collected, they were able to demonstrate that hybrid composites of graphitic carbon nitride and metal halide perovskites are interesting as valuable photocatalysts for the in-situ generation of ¹O₂ to perform HDA, ene, and oxidation reactions with suitable dienes and alkenes. At the same time, the group observed some limitations, especially in the case of acyclic alkene oxidation as well as poor chemoselectivity [42].

Corti et al. highlight that this is the first application of metal halide perovskites-based composites for the generation of singlet oxygen, leading to the development of a platform to

further expand the knowledge and applicability of this class of catalyst for photochemical reactions [42].

3. Lead-Free MHPs

There are few examples of the application of lead-free MHPs in photocatalysis, like the ones listed in Table 3, possibly due to some stability limitation of tin (the preferred substituent for Pb) and, in general, for the fact that expansion of lead-free materials to other fields in addition to photovoltaics is still in its infancy.

Table 3. Pb-free photocatalytic systems reviewed in the present paper highlighting the reaction, reaction yield, and illumination mean.

Catalyst	Reaction	Reaction Yield	Illumination	Reference
HDA ₂ SnI ₄ (HAD = hexadecylammonium)	Decarboxylation of indoline-2-carboxylic acid	30%	White LED	[39]
	Dehydrogenation of indoline-2-carboxylic acid	47%		
Cs ₃ Bi ₂ Br ₉	ring-opening of epoxides	Up to 88%	λ > 420 nm	[43]
Cs ₃ Bi ₂ Br ₉	Toluene oxidation	0.23%	Xe lamp (λ > 420 nm)	[44]
Cs ₃ Sb ₂ Br ₉	Toluene oxidation	-	λ > 420 nm	[45]
PEA ₂ SnBr ₄	¹ O ₂ hetero Diels-Alder cycloaddition reaction	26%	Simulated solar light	[42]
DMA ₂ SnBr ₃		63%		

HDA₂SnI₄ (HAD = hexadecylammonium) has been proposed by Hong et al. for photocatalytic decarboxylation and dehydrogenation reactions, exactly as in the previous section with HDA₂PbI₄ (see “bulk” section, Hong et al.) [39].

Perovskite derivative Cs₃Bi₂Br₉ has been applied for the photocatalyzed ring-opening reaction of epoxides [43]. In order to simplify the reaction conditions, the authors applied an in-situ synthesis, in which the perovskite is formed directly inside the solution, obtaining aggregated particles with sizes ranging 50–500 nm [43]. Hong et al. studied such a catalyst to perform the ring-opening of styrene oxide by isopropanol to produce 2-isopropoxy-2-phenylethanol, achieving 99% conversion and 86% yield, via a mechanism (Figure 6a) that involves the formation of a radical species, derived from iso-propanol, which reacts with the epoxide through the opening of the ring [43]. The group also tested the same reaction, varying the epoxide and alcohol obtaining similar results, and concluded that the conversion and selectivity of the reaction strongly depend on the steric hindrance of the reagents [43].

The same compounds have been employed by Dai et al. for the photocatalysis of the selective benzylic C-H bond activation [44]. The authors exploited mesoporous silica-supported Cs₃Bi₂Br₉ nanoparticles, with sizes 2–5 nm, and loadings from 5–40% weight. They studied toluene oxidation as a model reaction and managed to obtain good conversion rates and 90% selectivity towards benzaldehyde production with the 10% perovskite sample [44]. The group also determined that the reaction proceeds via a radical mechanism (Figure 6b,c) in which toluene interacts with the excited perovskite to produce a carbon radical, reacts with atmospheric oxygen to form benzylic acid, which lastly decomposes to form benzaldehyde and water [44].

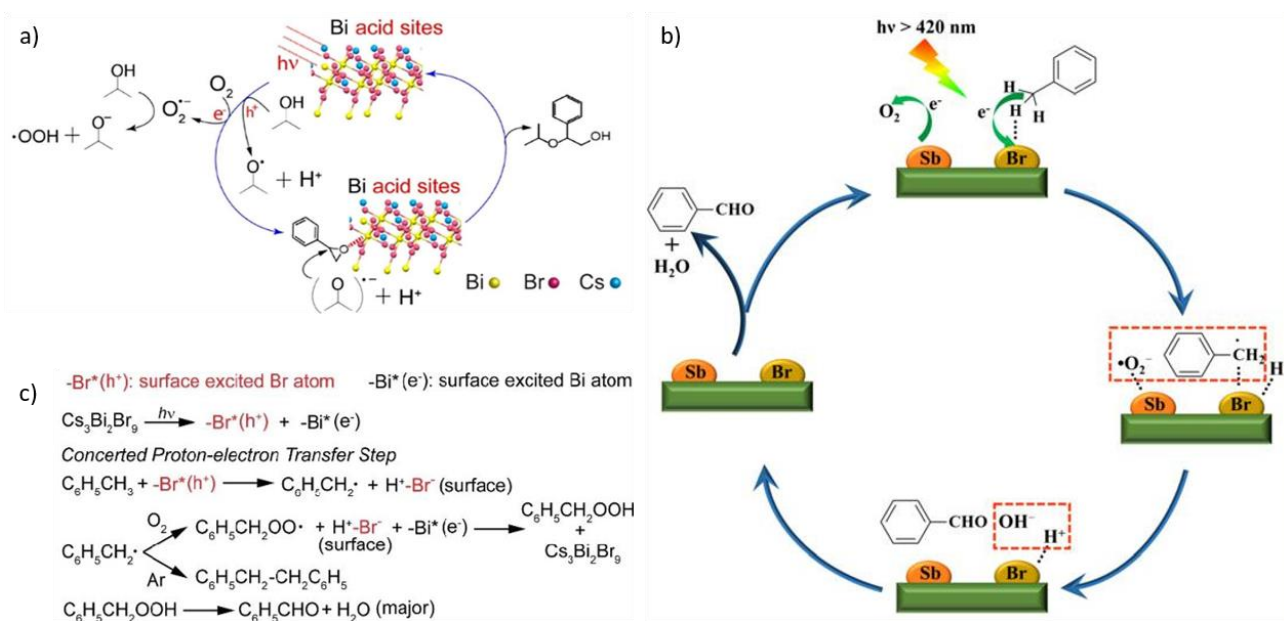


Figure 6. Proposed reaction mechanisms: (a) for the epoxyde alcoholysis reaction over $\text{Cs}_3\text{Bi}_2\text{Br}_9$. For details, see ref. [43]. Reprinted with permission from ref. [43]. Copyright 2019 ChemSusChem. (b,c) for the oxidation of toluene. For details, see refs. [44,45]. Reprinted with permission from refs. [44,45]. Copyright 2020 Angewandte Chemie International Edition. Copyright 2020 Angewandte Chemie International Edition.

Zhang et al. also performed photocatalytic toluene oxidation producing benzaldehyde by investigating NCs of $\text{Cs}_x\text{MA}_{3-x}\text{Sb}_2\text{Br}_9$ as catalyst [45]. They chose an anti-solvent method that only employs OA as ligand for the synthesis. The group also discovered that the samples of the solid solution with increasing Cs content are correspondingly more active towards the photocatalysis of the reaction [45]. The mechanism (Figure 6b,c) described is fairly similar to the previous one, however both toluene and atmospheric O_2 interact with the perovskite to form radicals, which then react to form benzaldehyde and OH^- , lastly producing H_2O by reaction with H^+ adsorbed onto the perovskite [45].

Finally, Corti et al. studied the coupling of a lead-free 2D/3D metal halide perovskite with $g\text{-C}_3\text{N}_4$ to create novel catalytic systems for sustainable singlet oxygen generation, namely, $g\text{-C}_3\text{N}_4/\text{PEA}_2\text{SnBr}_4$ and $g\text{-C}_3\text{N}_4/\text{DMASnBr}_3$ [42].

4. Conclusions

The possible use of MHPs as effective photocatalysts has become clear to the scientific community in the last few years. Bulk and nanocrystalline metal halide perovskites have been shown to be excellent semiconductors with suitable energy levels to run most of the key solar-driven reactions of current interest for solar fuels production [2]. This review summarized the current status of the application of MHPs in photocatalyzed organic syntheses/transformation which to date have shown, in most of the cases, significant advantages with respect to traditional photocatalysts. It is clear that the use of MHPs in this field is still in infancy and that more extended work, to widen the library of organic reactions where they can be advantageously applied, is still required. At the same time, rigorous mechanistic studies will reveal the advantages as well limitations of their use with respect to common catalytic systems. However, MHPs possess a unique capability of chemical structure and electronic properties tunability which will for sure allow finding optimal photocatalysts for most of the expected applications. The promising results reported so far allow us to predict a further growth of the branch in different directions: the testing of syntheses not reported yet by means of already known halide perovskite photocatalysts, the use of new phases with a significant focus on lead-free materials, and the exploitation of effective heterostructures to further improve the catalytic activity.

Author Contributions: All the authors contributed equally to the realizations of this work. All authors have read and agreed to the published version of the manuscript.

Funding: We acknowledge the support from RSE SpA.

Conflicts of Interest: The authors declare no conflict of interest.

References

1. Reischauer, S.; Pieber, B. Emerging Concepts in Photocatalytic Organic Synthesis. *iScience* **2021**, *24*, 102209. [[CrossRef](#)]
2. Zhu, X.; Lin, Y.; San Martin, J.; Sun, Y.; Zhu, D.; Yan, Y. Lead Halide Perovskites for Photocatalytic Organic Synthesis. *Nat. Commun.* **2019**, *10*, 2843. [[CrossRef](#)] [[PubMed](#)]
3. Romero, N.A.; Nicewicz, D.A. Organic Photoredox Catalysis. *Chem. Rev.* **2016**, *116*, 10075–10166. [[CrossRef](#)]
4. Prier, C.K.; Rankic, D.A.; MacMillan, D.W. Visible Light Photoredox Catalysis with Transition Metal Complexes: Applications in Organic Synthesis. *Chem. Rev.* **2013**, *113*, 5322–5363. [[CrossRef](#)]
5. Li, X.; Li, Z.; Gao, Y.; Meng, Q.; Yu, S.; Weiss, R.G.; Tung, C.; Wu, L. Mechanistic Insights into the Interface-directed Transformation of Thiols into Disulfides and Molecular Hydrogen by Visible-light Irradiation of Quantum Dots. *Angew. Chem.* **2014**, *126*, 2117–2121. [[CrossRef](#)]
6. Zhang, Z.; Edme, K.; Lian, S.; Weiss, E.A. Enhancing the Rate of Quantum-Dot-Photocatalyzed Carbon–Carbon Coupling by Tuning the Composition of the Dot’s Ligand Shell. *J. Am. Chem. Soc.* **2017**, *139*, 4246–4249. [[CrossRef](#)] [[PubMed](#)]
7. Cherevatskaya, M.; Neumann, M.; Fuldner, S.; Harlander, C.; Kümmel, S.; Dankesreiter, S.; Pfitzner, A.; Zeitler, K.; König, B. Visible-light-promoted Stereoselective Alkylation by Combining Heterogeneous Photocatalysis with Organocatalysis. *Angew. Chem. Int. Ed.* **2012**, *51*, 4062–4066. [[CrossRef](#)]
8. Nicewicz, D.A.; MacMillan, D.W. Merging Photoredox Catalysis with Organocatalysis: The Direct Asymmetric Alkylation of Aldehydes. *Science* **2008**, *322*, 77–80. [[CrossRef](#)]
9. Burschka, J.; Pellet, N.; Moon, S.-J.; Humphry-Baker, R.; Gao, P.; Nazeeruddin, M.K.; Grätzel, M. Sequential Deposition as a Route to High-Performance Perovskite-Sensitized Solar Cells. *Nature* **2013**, *499*, 316–319. [[CrossRef](#)]
10. Saparov, B.; Mitzi, D.B. Organic–Inorganic Perovskites: Structural Versatility for Functional Materials Design. *Chem. Rev.* **2016**, *116*, 4558–4596. [[CrossRef](#)]
11. Zhu, X.; Lin, Y.; Sun, Y.; Beard, M.C.; Yan, Y. Lead-Halide Perovskites for Photocatalytic α -Alkylation of Aldehydes. *J. Am. Chem. Soc.* **2019**, *141*, 733–738. [[CrossRef](#)] [[PubMed](#)]
12. Mao, L.; Stoumpos, C.C.; Kanatzidis, M.G. Two-Dimensional Hybrid Halide Perovskites: Principles and Promises. *J. Am. Chem. Soc.* **2018**, *141*, 1171–1190. [[CrossRef](#)] [[PubMed](#)]
13. Yang, Y.; Yang, M.; Moore, D.T.; Yan, Y.; Miller, E.M.; Zhu, K.; Beard, M.C. Top and Bottom Surfaces Limit Carrier Lifetime in Lead Iodide Perovskite Films. *Nat. Energy* **2017**, *2*, 16207. [[CrossRef](#)]
14. Yang, Y.; Ostrowski, D.P.; France, R.M.; Zhu, K.; Van De Lagemaat, J.; Luther, J.M.; Beard, M.C. Observation of a Hot-Phonon Bottleneck in Lead-Iodide Perovskites. *Nat. Photonics* **2016**, *10*, 53–59. [[CrossRef](#)]
15. Dong, Q.; Fang, Y.; Shao, Y.; Mulligan, P.; Qiu, J.; Cao, L.; Huang, J. Electron-Hole Diffusion Lengths > 175 Mm in Solution-Grown CH₃NH₃PbI₃ Single Crystals. *Science* **2015**, *347*, 967–970. [[CrossRef](#)]
16. Xu, Y.-F.; Yang, M.-Z.; Chen, B.-X.; Wang, X.-D.; Chen, H.-Y.; Kuang, D.-B.; Su, C.-Y. A CsPbBr₃ Perovskite Quantum Dot/Graphene Oxide Composite for Photocatalytic CO₂ Reduction. *J. Am. Chem. Soc.* **2017**, *139*, 5660–5663. [[CrossRef](#)]
17. Chen, K.; Deng, X.; Dodekatos, G.; Tüysüz, H. Photocatalytic Polymerization of 3,4-Ethylenedioxythiophene over Cesium Lead Iodide Perovskite Quantum Dots. *J. Am. Chem. Soc.* **2017**, *139*, 12267–12273. [[CrossRef](#)]
18. Wong, Y.; De Andrew Ng, J.; Tan, Z. Perovskite-initiated Photopolymerization for Singly Dispersed Luminescent Nanocomposites. *Adv. Mater.* **2018**, *30*, 1800774. [[CrossRef](#)]
19. Wu, W.-B.; Wong, Y.-C.; Tan, Z.-K.; Wu, J. Photo-Induced Thiol Coupling and C–H Activation Using Nanocrystalline Lead-Halide Perovskite Catalysts. *Catal. Sci. Technol.* **2018**, *8*, 4257–4263. [[CrossRef](#)]
20. Zhao, Y.; Zhu, K. Organic–Inorganic Hybrid Lead Halide Perovskites for Optoelectronic and Electronic Applications. *Chem. Soc. Rev.* **2016**, *45*, 655–689. [[CrossRef](#)]
21. Romani, L.; Malavasi, L. Solar-Driven Hydrogen Generation by Metal Halide Perovskites: Materials, Approaches, and Mechanistic View. *ACS Omega* **2020**, *5*, 25511–25519. [[CrossRef](#)]
22. Feng, A.; Jiang, X.; Zhang, X.; Zheng, X.; Zheng, W.; Mohammed, O.F.; Chen, Z.; Bakr, O.M. Shape Control of Metal Halide Perovskite Single Crystals: From Bulk to Nanoscale. *Chem. Mater.* **2020**, *32*, 7602–7617. [[CrossRef](#)]
23. González-Carrero, S.; Galian, R.E.; Pérez-Prieto, J. Organometal Halide Perovskites: Bulk Low-Dimension Materials and Nanoparticles. *Part. Part. Syst. Character.* **2015**, *32*, 709–720. [[CrossRef](#)]
24. Pisanu, A.; Quadrelli, P.; Malavasi, L. Facile Anion-Exchange Reaction in Mixed-Cation Lead Bromide Perovskite Nanocrystals. *RSC Adv.* **2019**, *9*, 13263–13268. [[CrossRef](#)]
25. Pisanu, A.; Ferrara, C.; Quadrelli, P.; Guizzetti, G.; Patrini, M.; Milanese, C.; Tealdi, C.; Malavasi, L. The FA_{1-x}MA_xPbI₃ System: Correlations among Stoichiometry Control, Crystal Structure, Optical Properties, and Phase Stability. *J. Phys. Chem. C* **2017**, *121*, 8746–8751. [[CrossRef](#)]

26. Lu, H.; Zhu, X.; Miller, C.; Martin, J.S.; Chen, X.; Miller, E.M.; Yan, Y.; Beard, M.C. Enhanced Photoredox Activity of CsPbBr₃ Nanocrystals by Quantitative Colloidal Ligand Exchange. *J. Chem. Phys.* **2019**, *151*, 204305. [[CrossRef](#)] [[PubMed](#)]
27. Wang, K.; Lu, H.; Zhu, X.; Lin, Y.; Beard, M.C.; Yan, Y.; Chen, X. Ultrafast Reaction Mechanisms in Perovskite Based Photocatalytic C–C Coupling. *ACS Energy Lett.* **2020**, *5*, 566–571. [[CrossRef](#)]
28. Rosa-Pardo, I.; Casadevall, C.; Schmidt, L.; Claros, M.; Galian, R.E.; Lloret-Fillol, J.; Perez-Prieto, J. The Synergy between the CsPbBr₃ Nanoparticle Surface and the Organic Ligand Becomes Manifest in a Demanding Carbon–Carbon Coupling Reaction. *ChemComm* **2020**, *56*, 5026–5029. [[CrossRef](#)] [[PubMed](#)]
29. Shi, T.; Sun, K.; Chen, X.-L.; Zhang, Z.-X.; Huang, X.-Q.; Peng, Y.-Y.; Qu, L.-B.; Yu, B. Recyclable Perovskite as Heterogeneous Photocatalyst for Aminomethylation of Imidazo-Fused Heterocycles. *Adv. Synth. Catal.* **2020**, *362*, 2143–2149. [[CrossRef](#)]
30. Peng, Y.; Albero, J.; García, H. Surface Silylation of Hybrid Benzidinium Lead Perovskite and Its Influence on the Photocatalytic Activity. *ChemCatChem* **2019**, *11*, 6384–6390. [[CrossRef](#)]
31. Schünemann, S.; van Gastel, M.; Tüysüz, H. A CsPbBr₃/TiO₂ Composite for Visible-Light-Driven Photocatalytic Benzyl Alcohol Oxidation. *ChemSusChem* **2018**, *11*, 2057–2061. [[CrossRef](#)] [[PubMed](#)]
32. Zhu, E.; Zhao, Y.; Dai, Y.; Wang, Q.; Dong, Y.; Chen, Q.; Li, Y. Heterojunction-Type Photocatalytic System Based on Inorganic Halide Perovskite CsPbBr₃. *Chin. J. Chem.* **2020**, *38*, 1718–1722. [[CrossRef](#)]
33. Huang, H.; Yuan, H.; Janssen, K.P.F.; Solís-Fernández, G.; Wang, Y.; Tan, C.Y.X.; Jonckheere, D.; Debroye, E.; Long, J.; Hendrix, J.; et al. Efficient and Selective Photocatalytic Oxidation of Benzylic Alcohols with Hybrid Organic–Inorganic Perovskite Materials. *ACS Energy Lett.* **2018**, *3*, 755–759. [[CrossRef](#)]
34. Huang, H.; Yuan, H.; Zhao, J.; Solís-Fernández, G.; Zhou, C.; Seo, J.W.; Hendrix, J.; Debroye, E.; Steele, J.A.; Hofkens, J.; et al. C(Sp³)–H Bond Activation by Perovskite Solar Photocatalyst Cell. *ACS Energy Lett.* **2019**, *4*, 6. [[CrossRef](#)]
35. Qiu, P.; Wang, Q.; Zhao, Y.; Dai, Y.; Dong, Y.; Chen, C.; Chen, Q.; Li, Y. Fabricating Surface-Functionalized CsPbBr₃/Cs₄PbBr₆ Nanosheets for Visible-Light Photocatalytic Oxidation of Styrene. *Front. Chem.* **2020**, *8*, 130. [[CrossRef](#)]
36. Li, Y.; Shu, Q.; Du, Q.; Dai, Y.; Zhao, S.; Zhang, J.; Li, L.; Chen, K. Surface Modification for Improving the Photocatalytic Polymerization of 3,4-Ethylenedioxythiophene over Inorganic Lead Halide Perovskite Quantum Dots. *ACS Appl. Mater. Interfaces* **2020**, *12*, 451–460. [[CrossRef](#)]
37. Zhu, Y.; Liu, Y.; Miller, K.A.; Zhu, H.; Egap, E. Lead Halide Perovskite Nanocrystals as Photocatalysts for PET-RAFT Polymerization under Visible and Near-Infrared Irradiation. *ACS Macro Lett.* **2020**, *9*, 725–730. [[CrossRef](#)]
38. Protesescu, L.; Yakunin, S.; Bodnarchuk, M.I.; Krieg, F.; Caputo, R.; Hendon, C.H.; Yang, R.X.; Walsh, A.; Kovalenko, M.V. Nanocrystals of Cesium Lead Halide Perovskites (CsPbX₃, X = Cl, Br, and I): Novel Optoelectronic Materials Showing Bright Emission with Wide Color Gamut. *Nano Lett.* **2015**, *15*, 3692–3696. [[CrossRef](#)]
39. Hong, Z.; Chong, W.K.; Ng, A.Y.R.; Li, M.; Ganguly, R.; Sum, T.C.; Soo, H.S. Hydrophobic Metal Halide Perovskites for Visible-Light Photoredox C–C Bond Cleavage and Dehydrogenation Catalysis. *Angew. Chem. Int. Ed.* **2019**, *58*, 3456–3460. [[CrossRef](#)]
40. Zhang, M.; Li, Z.; Xin, X.; Zhang, J.; Feng, Y.; Lv, H. Selective Valorization of 5-Hydroxymethylfurfural to 2,5-Diformylfuran Using Atmospheric O₂ and MAPbBr₃ Perovskite under Visible Light. *ACS Catal.* **2020**, *10*, 14793–14800. [[CrossRef](#)]
41. Dong, Y.; Li, K.; Luo, W.; Zhu, C.; Guan, H.; Wang, H.; Wang, L.; Deng, K.; Zhou, H.; Xie, H.; et al. The Role of Surface Termination in Halide Perovskites for Efficient Photocatalytic Synthesis. *Angew. Chem. Int. Ed.* **2020**, *59*, 12931–12937. [[CrossRef](#)] [[PubMed](#)]
42. Corti, M.; Chiara, R.; Romani, L.; Mannucci, B.; Malavasi, L.; Quadrelli, P. G-C₃N₄/Metal Halide Perovskite Composites as Photocatalysts for Singlet Oxygen Generation Processes for the Preparation of Various Oxidized Synthons. *Catal. Sci. Technol.* **2021**, *11*, 2292–2298. [[CrossRef](#)]
43. Dai, Y.; Tüysüz, H. Lead-Free Cs₃Bi₂Br₉ Perovskite as Photocatalyst for Ring-Opening Reactions of Epoxides. *ChemSusChem* **2019**, *12*, 2587–2592. [[CrossRef](#)] [[PubMed](#)]
44. Dai, Y.; Poidevin, C.; Ochoa-Hernández, C.; Auer, A.A.; Tüysüz, H. A Supported Bismuth Halide Perovskite Photocatalyst for Selective Aliphatic and Aromatic C–H Bond Activation. *Angew. Chem. Int. Ed.* **2020**, *59*, 5788–5796. [[CrossRef](#)] [[PubMed](#)]
45. Zhang, Z.; Yang, Y.; Wang, Y.; Yang, L.; Li, Q.; Chen, L.; Xu, D. Revealing the A-Site Effect of Lead-Free A₃Sb₂Br₉ Perovskite in Photocatalytic C(Sp³)–H Bond Activation. *Angew. Chem.* **2020**, *132*, 18293–18296. [[CrossRef](#)]